Available online at www.sciencedirect.com

ScienceDirect

Ceramics International 39 (2013) 8805–8813

CERAMICS INTERNATIONAL

www.elsevier.com/locate/ceramint

Comparison of microstructure and mechanical properties of plasma-sprayed nanostructured and conventional yttria stabilized zirconia thermal barrier coatings

Reza Ghasemi*, Reza Shoja-Razavi, Reza Mozafarinia, Hossein Jamali

Department of Materials Engineering, Malek-Ashtar University of Technology, Shahinshahr, Isfahan, Iran

Received 5 April 2013; received in revised form 18 April 2013; accepted 19 April 2013
Available online 7 May 2013

Abstract

The main goal of this paper was to evaluate and compare the microstructure and mechanical properties of plasma-sprayed nanostructured and conventional yttria stabilized zirconia (YSZ) thermal barrier coatings (TBCs). To this end, NiCrAlY bond coat, nanostructured, and conventional YSZ coatings were deposited on Inconel 738LC substrate by atmospheric plasma spraying (APS). The mechanical properties of the coating were evaluated using nanoindentation and bonding strength tests. The microstructure and phase composition of the coating were characterized by field emission scanning electron microscopy (FESEM) and X-ray diffractometry (XRD). The nanostructured YSZ coating contained both nanosized particles retained from the powder and microcolumnar grains formed through the resolidification of the molten part of the powder, whereas the microstructure of the conventional YSZ coating consisted of columnar grain splats only. The phase composition of the as-sprayed nanostructured coating consisted of the non-transformable tetragonal phase, while the conventional coating showed the presence of both the monoclinic and non-transformable tetragonal phases. The results of nanoindentation and bonding strength tests indicated that the mechanical properties of the nanostructured coating were better than those of the conventional coating.

Keywords: C. Mechanical properties; Thermal barrier coating; Microstructure; Atmospheric plasma spraying

1. Introduction

Plasma-sprayed thermal barrier coating system is widely used in turbine engines to allow a higher turbine entry temperature (which increases the thermal efficiency of the gas turbine) or to achieve a lower substrate temperature [1–4]. The TBC system consists of a superalloy substrate, bond coat layer, and a heat insulating ceramic top coat layer [5,6]. The bond coat typically consists of MCrAlY, where M is a metal such as Ni and/or Co. The primary role of the bond coat in a TBC system is to provide good adhesion between the metal substrate and the ceramic top coat, while giving good oxidation protection to the underlying substrate alloy [7–9]. Zirconium oxide (ZrO_2, Zirconia) coatings were commonly used as the top coat because of low thermal conductivity, high temperature stability in oxidizing and combustion atmospheres, and the high coefficient of thermal expansion [10–12]. A thermally grown oxide (TGO) is formed at the interface between the bond coat and ceramic top coat due to high temperature oxidation of the bond coat. The TGO consists of aluminum oxide, at least initially [13–15].

Two basic process technologies now widely adopted to deposit thermal barrier coatings are plasma spraying or electron beam physical vapor deposition (EB-PVD). EB-PVD is often favored over plasma deposition for TBCs on turbine airfoils since it applies a smooth surface of better aerodynamic quality with less interference with cooling holes. However, the widely used plasma spray process has benefits, including a lower application cost, an ability to coat a greater diversity of components with a wider composition range, and a large installed equipment base [16–18].

The mechanical properties of a coating depend on several factors such as (i) spray process and its parameters, (ii) properties

*Corresponding author. Tel.: +98 3125225041; fax: +98 3125228530.
E-mail addresses: r_ghasemi@mut-es.ac.ir, reza.ghasemi65@gmail.com (R. Ghasemi).

0272-8842/$ - see front matter © 2013 Elsevier Ltd and Techna Group S.r.l. All rights reserved.
http://dx.doi.org/10.1016/j.ceramint.2013.04.068

of the particles, especially their morphologies and (iii) microstructure of the coating and their anisotropic character [19,20]. Also, quality and further performance of a TBC are strongly dependent on the adhesion between the coating and the substrate [21,22]. Therefore, considering mechanical properties and adhesive strength is essential to improve the reliability and lifetime performance of the APS-TBC system. Nanoindentation test is a novel technique that has been adopted by some researchers recently to evaluate the mechanical properties of coatings system [23–26]. A widely used and accepted adhesion test is the tensile adhesion test according to the ASTM-C633 standard [21,22,27].

In recent years, studies on the characterization of nanostructured coatings have become an active field of academic research and industrial application because of the extraordinary properties of nanostructured coating when compared to the conventional coating. It was reported that nanostructured YSZ coatings had low thermal conductivity [4,28], high coefficient of thermal expansion [29,30], and excellent mechanical properties [1,31] when compared to YSZ conventional coatings. Therefore, nanostructured TBCs are expected to provide better performance than the conventional coatings. Even though the study of nanostructured YSZ coatings is not new and there are a lot of reports in literature, but some interesting results are obtained in this paper.

In this study, nanostructured and conventional YSZ TBCs were prepared using the atmospheric plasma spraying process. The microstructure, phase composition, and mechanical properties of the plasma-sprayed nanostructured TBCs were investigated and compared with those of the conventional TBCs.

2. Materials and methods

2.1. Material

A Ni-based superalloy (Inconel 738LC, the composition of which is summarized in Table 1) was used as the substrate material. Before thermal spraying, the substrate surface was grit-blasted with alumina abrasive powder of 24 mesh, under a pressure of 5 bar and a distance of 10 cm. The surface was then cleaned with acetone and preheated using negative transferred arc to provide optimum substrate bonding to the coating. A commercially available NiCrAlY powder (AMDRY 962, Sulzer Metco Inc., USA) with nominal composition of Ni–22Cr–10Al–1.0Y(wt%) was used for spraying the bond coat of TBCs. The spherical powders were gas atomized and the particles size was 56–106 μm, as shown in Fig. 1(a). Two kinds of nanostructured and conventional YSZ powders were used as feedstock for the top coat. The conventional YSZ powder was Metco 204NS (Sulzer Metco, Westbury, NY) with nominal composition of ZrO_2–8 wt%Y_2O_3 and the particles

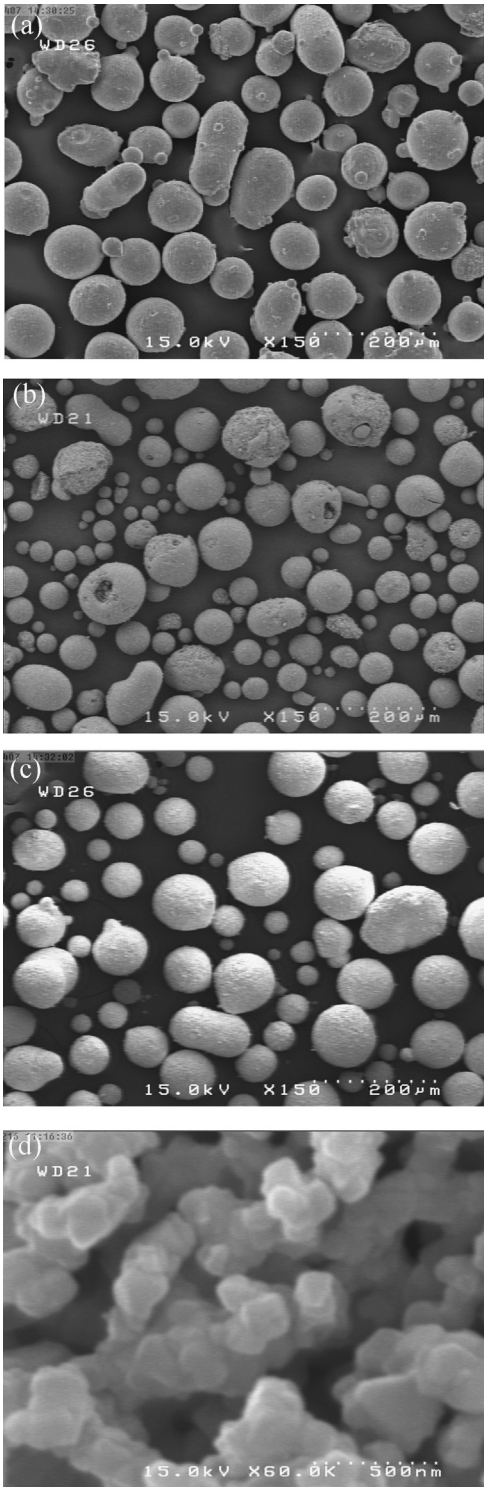

Fig. 1. FESEM micrographs of starting powders: (a) NiCrAlY powder, (b) conventional YSZ powder, (c) agglomerated nanostructured YSZ powder particle and (d) particle of (c) observed at a higher magnification, showing individual nanosized YSZ particles.

Table 1
Chemical composition of Inconel 738LC.

Element	Cr	Co	Mo	W	Al	Ti	Ta	Nb	C	B	Zr	Ni
wt%	16.00	8.50	1.75	2.60	3.40	3.40	1.70	0.009	0.11	0.01	0.05	61.58

size was 11–125 μm, as shown in Fig. 1(b). The nanostructured powder used for top coat consisted of commercial ZrO_2–7 wt%Y_2O_3 (Nanox S4007, Inframet Corp., Farmington, CT) spherical particles with size ranging from 15 to 150 μm in diameter, as shown in Fig. 1(c). Also, as shown Fig. 1(d), this powder consisted of agglomerated nanosized particles.

2.2. Air plasma spraying

The plasma spraying was carried out using a Metco A3000S atmospheric plasma spray system with F4-MB plasma gun (Sulzer Metco AG, Switzerland). The feedstock powders were fed with Twin-system 10-C. A mixture of gas argon and hydrogen was used as the working gases for forming plasma. Ar stabilized arc inside a nozzle and H_2 provided increased enthalpy and higher plasma temperature. Also, Ar gas was used as the carrier gas for transferring the powder particles of the powder supply to the plasma torch. During spraying, the substrate and coatings were cooled using compressed air. The spraying parameters are listed in Table 2.

2.3. Bonding strength test

The as-sprayed coatings were subjected to bonding strength using ASTM-C633 standard test method for adhesion or cohesion strength of thermal spray coatings. The method involved fastening the sample covered to the sample uncoated using SW 2214 epoxy adhesive (3M Scotch-weld, bond strength ~70 MPa), which was self-adhesive at 140 °C for 2 h. Then samples were loaded with a loading rate of 5 mm/min until fracture and the corresponding fracture stress were recorded. The final value represented the average value of 5 samples sprayed with the same parameters.

2.4. Nanoindentation test

Nanoindentation test is a useful method to study Young's modulus (E) and hardness (H) of the coatings. Nanoindentation test was carried out on polished cross-section using a Nanoindentation Compact Platform with Berkovich indenter. The maximum load was 10 mN in the experiment, loading rate was 20 mN/min, unloading rate was 20 mN/min, and dwell period at maximum load was 30 s.

Table 2
Parameters of plasma spraying.

Parameter	NiCrAlY	Conventional YSZ	Nanostructured YSZ
Current (A)	600	500	600
Voltage (V)	75	80	72
Primary gas, Ar (SLPM[a])	65	35	35
Secondary gas, H_2 (SLPM)	14	12	10
Carrier gas, Ar (SLPM)	2.3	2.6	3.5
Powder feed rate (g/min)	40	20	18
Spray distance (mm)	120	120	120

[a]Standard liter per minute.

2.5. Specimens characterization

The phase compositions of YSZ powders and the as-sprayed coatings were analyzed by an X-ray diffraction XRD (D8 ADVANCE, Bruker, Germany) using CuKα radiation (λ=0.15406 nm) produced at 40 KV and 40 mA. The analyzed range of the diffraction angle 2θ was between 20° and 90°, by step width of 0.03° and a time per step equal to 1 s. The morphology of NiCrAlY and YSZ powders and the microstructure of coatings were determined using field emission scanning electron microscope (FESEM, S-4160, Hitachi, Japan), which operated under low accelerating voltage conditions. The surface roughness (R_a) of YSZ coating was measured by a Mitutoyo Surftest profilometer (Mitutoyo SJ-201P, Japan) with a cut-off length of 800 μm and a measurement length of 4 mm. The roughness reported was the average of five values scanned from different areas on the coating surface.

3. Results and discussion

3.1. Coating microstructure

The FESEM of polished cross-section of the as-sprayed conventional coating is shown in Fig. 2(a). It is composed of a 230 ± 25 μm thick YSZ top coat and a bond coat with the thickness of 190 ± 25 μm. It can be seen that no visible stratified structure is observed in coating layers, indicating the better structural integration of the TBC system. The interface between the ceramic and bond coat is rough. This surface includes small, almost free standing peninsular metal deposits which penetrate relatively deeply and are surrounded by ceramic. This feature creates angles and pockets that promote mechanical interlocking between the ceramic and the bond coat [32,33].

Fig. 2(b) shows the FESEM image of the microstructure of the as-sprayed conventional coating found in fractured cross-section. It can be seen that there are typical lamellar structures with columnar grains which enclose transverse microcracks and porosity. In the thermal spraying process, the powder particles are completely melted in the transit between the injection point and the substrate surface. The molten particles then strike the substrate surface, where they are flattened and solidified to form splat. In fact, molten particles acquire the same lenticular shape over previously piled-up solidified splats. So the coatings develop a lamellar structure parallel to the interface. The lamellae exhibit a characteristic columnar structure formed by directional solidification at the cooling rate [32,34,35]. Also, the presence of intra-splat crack, inter-splat crack, voids, and pores within the splat is shown in Fig. 2(c). The formation of intra-splat cracks in the splat structure is due to the disability of the particles to contract independently from their neighbors during the solidification process. However, adhesion among the splats is significantly different from that with the metallic substrate, inter-splat crack form at the splat boundaries because of the relatively weak adhesion [32,36–38]. The presence of the inter-splat crack has a significant effect on the TBC thermal conductivity and thermal

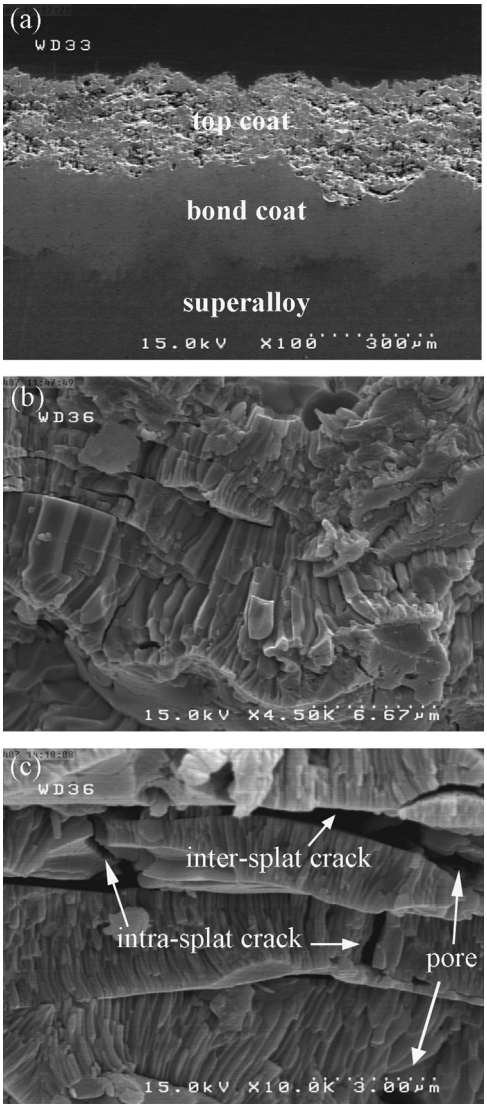

Fig. 2. FESEM micrographs of (a) polished cross-section of TBC with conventional YSZ top coat, (b) fractured cross-section of conventional YSZ coating and (c) columnar grains within the splats.

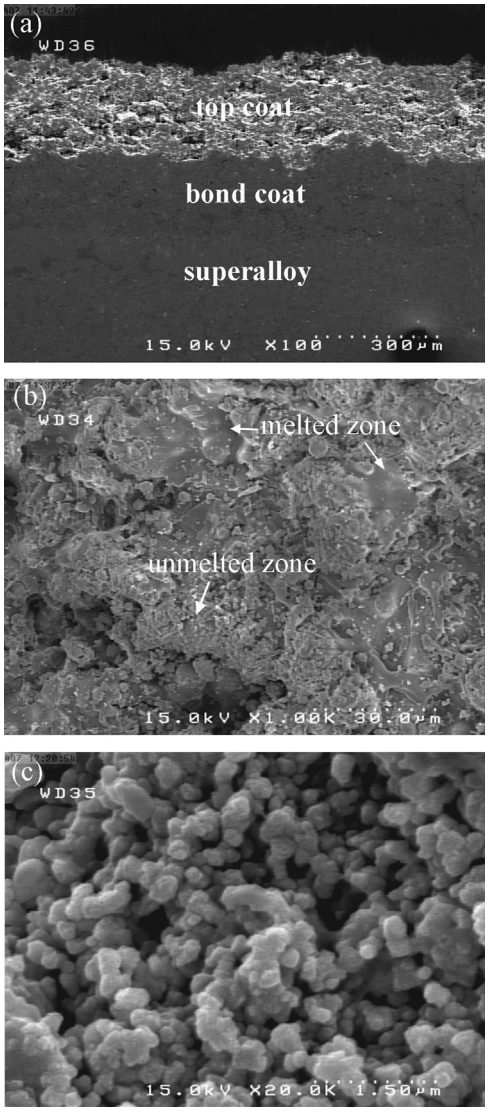

Fig. 3. FESEM micrographs of (a) polished cross-section of TBC with nanostructured YSZ top coat, (b) top surface of the nanostructured coating and (c) partially molted zone of (b) at a higher magnification.

shock resistance [39,40]. The presence of voids and pores is due to the lack of complete overlap of adjacent splat and entrapment of the air during the plasma spraying [36,41].

Fig. 3(a) shows the FESEM image of the polished cross-section of the as-sprayed nanostructured coating. It can be seen that the density of top coat for nanostructured TBCs is significantly higher than that of the conventional TBCs. According to the image, the cracks and pores in nanostructured coatings are relatively finer and fewer. This can be attributed to the refined grains of nanostructured coating and the increasing toughness [42]. Fig. 3(b) presents the surface morphology of the as-sprayed nanostructured coating, showing two kinds of structure. One is the continuous molten phase, similar to the conventional as-sprayed coating, and the other is non-molten and partially molten phase that retains the nanostructure of the starting powder. The surface roughness (R_a) of nanostructured coating was about 9.20 µm, which was significantly bigger than that of conventional coating (7.12 µm) at the same conditions, because partially molten particles involved in lower deformation impact the surface as compared to fully molten particles [36,43,44]. The melted zone of the top coat surface contains microcrack networks that are due to primary cooling stresses developed when the deposited particles are cooled from above the melting temperature to the substrate contact temperature. It relates to the increase of the roughness of the nanostructured coating [32,34]. Fig. 3(c) shows the non-melted and partially molten zones of Fig. 3(b) at a higher magnification, similar to the starting powder.

Fig. 4 shows the fractured cross-section of nanostructured YSZ coating at two magnifications. It can be seen from Fig. 4 (a) that there are two kinds of structures in the coating. One is that microcolumnar grain structures in the coating evolved from the resolidification of the molten part of the powder. On the other hand, the nanosized powder in the coating results

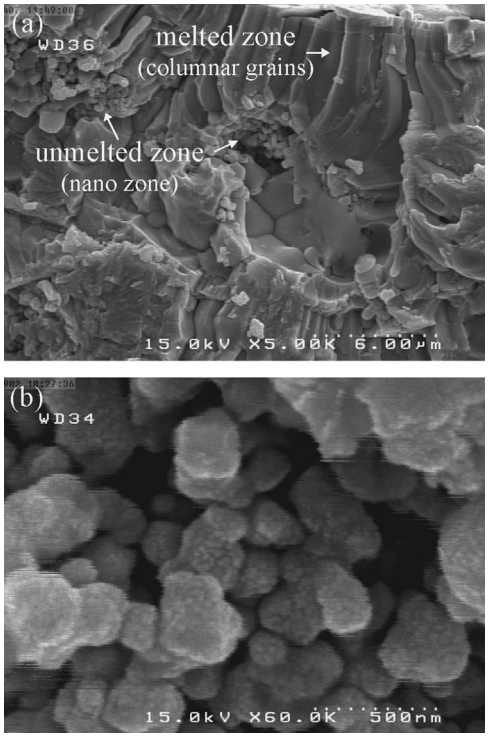

Fig. 4. FESEM micrographs of (a) fractured cross-section of nanostructured YSZ coating and (b) non-molten nanoparticles within coating at a high magnification.

from non-molten or partially molten part of the powders bonded by the molten part [45–47]. Fig. 4(b) shows that the initial nanostructure of powder remains in the coating. This zone is called nanozone. It can be seen that the morphology of the nanozone is similar to the morphology of the nanostructured YSZ powder (Fig. 1(d)). Nanozone is porous because the molten part of agglomerated partially molten particles is not fully infiltrated into non-molten core during thermal spraying. The presence of nanozone in the coating affirms the nanostructured coating. In order to maintain nanozone in the coating, it is necessary to avoid full melting of nanostructured agglomerated feedstock particle during the thermal spraying. Accordingly, the spraying parameters were optimized to partially melt the powder particles during plasma spraying. Also, the size of powder particles is very important. The coarse particles in low temperature region plasma plume tended to partially melt with an unmelted core due to its large mass and volume. The small powder at relatively high temperature was fully melted [32,34].

3.2. Phase analysis

Fig. 5 shows the X-ray diffraction patterns of the conventional and nanostructured YSZ powders and as-sprayed coatings. According to XRD patterns shown in Fig. 5(a), the conventional feedstock exhibits the presence of non-transformable tetragonal (T') phase of zirconia with a small amount of monoclinic phase. The conventional coating predominately consisted of a non-transformable tetragonal phase, but very weak diffraction peaks of monoclinic phase could be detected from coating. During plasma spraying, there were some partially molten particles forming the small amount of monoclinic phase. It should be noted the T' phase is typically of plasma sprayed zirconia, which is formed due to quenching of droplets at the substrate. The non-transformable tetragonal phase can be distinguished from the transformable tetragonal phase (T) with respect to the martensitic transformation to the monoclinic phase of zirconia [32,48,49]. It can be seen from Fig. 5(b) that there was no new phase in the coating and no clear difference of the diffraction pattern between the nanostructured YSZ powder and the as-sprayed coating was observed. So both powder and coating consisted of non-transformable tetragonal phase. The formation of T' phase in the nanostructured coating may be due to two factors: (i) the YSZ coating fabricated from nanostructured powder contained only T' phase, because the molten part of powder, due to rapid cooling, formed T' phase and non-molten part retained the T' phase; (ii) the Y_2O_3 content of YSZ was high enough, around 10 wt%, to increase the stabilization of the ZrO_2 high temperature phase upon cooling. So phase diagram of the ZrO_2–Y_2O_3 (Fig. 6) was the certification for the expression [32,50–52].

3.3. Bonding strength

The bonding strength test described here is similar to ASTM-C633 method. The tensile strength is obtained from the division of the maximum load applied at rupture by the cross-section area. The adhesion strength of the coating is given if the failure occurs at bond coat – substrate or top coat – bond coat interface. The cohesive strength of the coating is given if rupture is completely within the coating [19,53]. Two modes of failure were observed in this test, as shown in Fig. 7(a) failure in the glued joint between steel bar and top coat (Fig. 7(a and b) failure in the top coat – bond coat and bond coat – substrate interface (Fig. 7(b)). The results of the first failure mode are disregarded. The results and mode of coating failures in the test are described in Table 3. The most important mechanism of sprayed coatings adhesion is mechanical interlocking of the splats to roughness of the substrate. Epitaxy is the second mechanism that can occur if the sprayed material has the same or similar crystal structure [19,21,32]. Hence, the bonding strength between the cognate splats (cohesive strength) is higher than the non-cognate splats (adhesion strength). Accordingly, it can be seen from Fig. 7(b) that, generally, the coating failure location is at the interface between bond coat and top coat. This means an adhesive failure.

The nanostructured TBC exhibits an average bonding strength approximately 1.5 times higher when compared to the conventional TBC. The higher bonding strength of the nanostructured TBC, as compared to the conventional TBC, can be attributed to the coating microstructure. In conventional TBC, cracks extend to the splat boundaries without any hindrance. For nanostructured TBC with a bimodal microstructure, crack propagation could be interrupted by the non-molten or partially molten particles (nanozone), thereby increasing the bonding strength of the nanostructured coating [27,47,54].

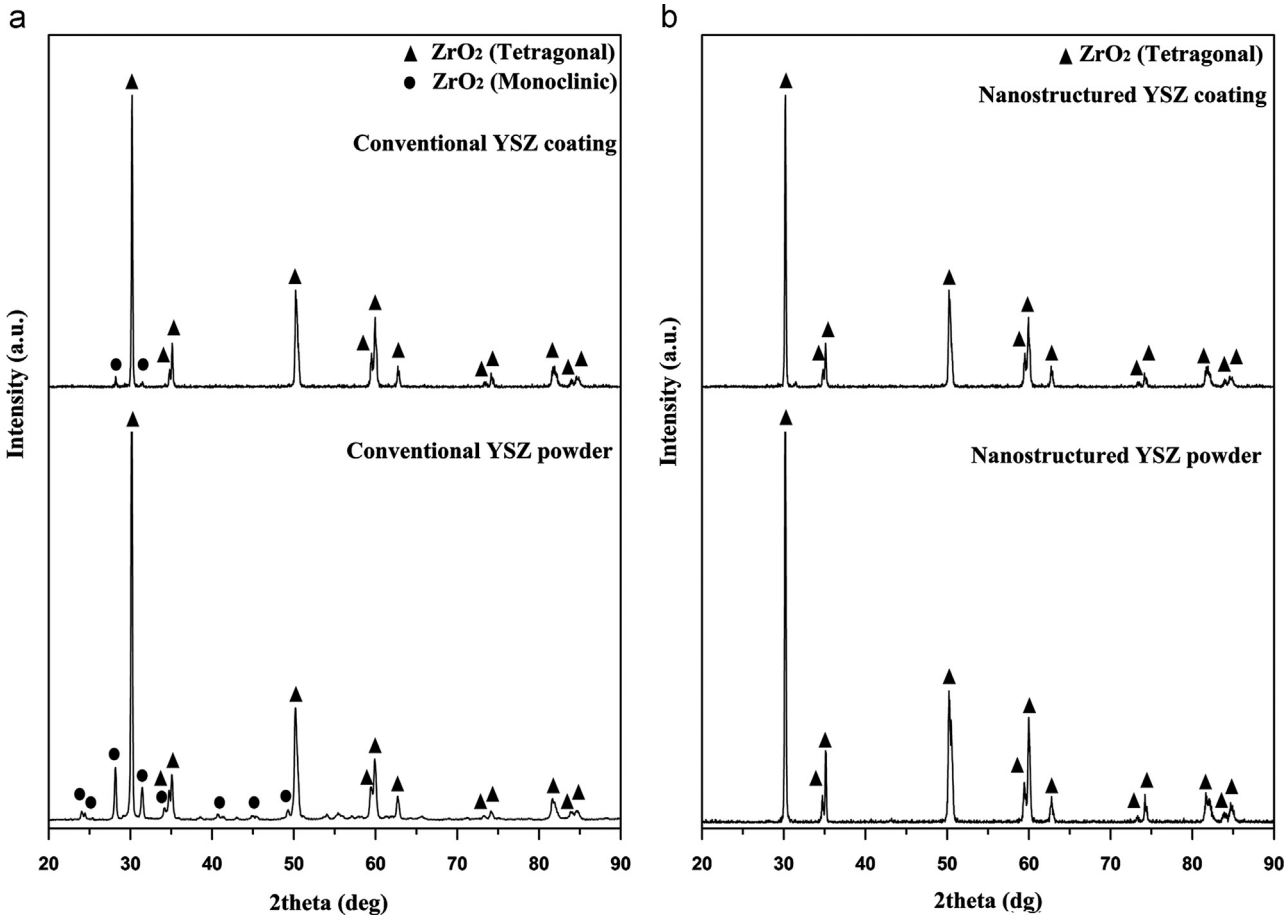

Fig. 5. XRD patterns of powder and coating of (a) conventional and (b) nanostructured YSZ.

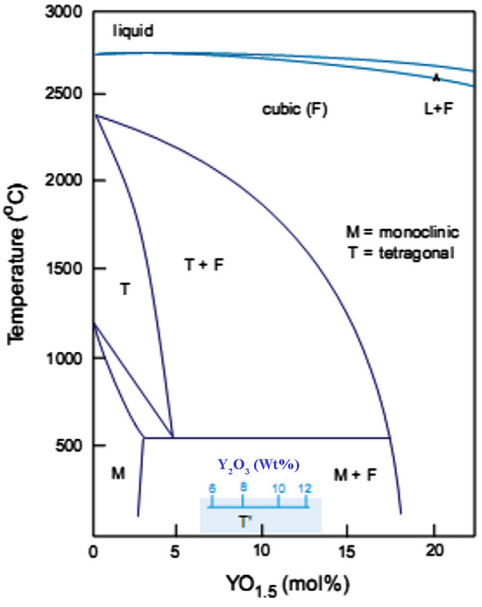

Fig. 6. Yttria–zirconia phase diagram.

3.4. Mechanical properties

Hardness and elastic modulus are two important parameters which help to evaluate mechanical properties of TBC for their durability. Fig. 8 shows load–displacement (P–h) curves obtained from conventional and nanostructured coatings. Table 4 summarizes the maximum value of the three items of the penetration depth, h_{max}, measured at peak load, P_{max}.

The slope of the curve, dP/dh, upon unloading, is indicative of the stiffness, S, of the contact. This value generally includes a contribution from both the material being tested and the response of the test device itself. The stiffness of the contact can be used to calculate the reduced Young's modulus E_r:

$$E_r = \frac{1}{\beta}\frac{\sqrt{\pi}}{2}\frac{S}{\sqrt{A}} \tag{1}$$

where the correction factor $\beta = 1.034$ is for a Berkovich tip, and A is the actual contact area in terms of contact depth that can be expressed as

$$A = 24.5h_c^2 \tag{2}$$

The reduced modulus, E_r, is related to Young's modulus, E_s, of the test specimen through the following relationship from contact mechanics:

$$\frac{1}{E_r} = \frac{(1-\vartheta_i^2)}{E_i} + \frac{(1-\vartheta_s^2)}{E_s} \tag{3}$$

Here, the subscript i indicates a property of the indenter material and the ϑ is Poisson's ratio. For the *diamond* indenter

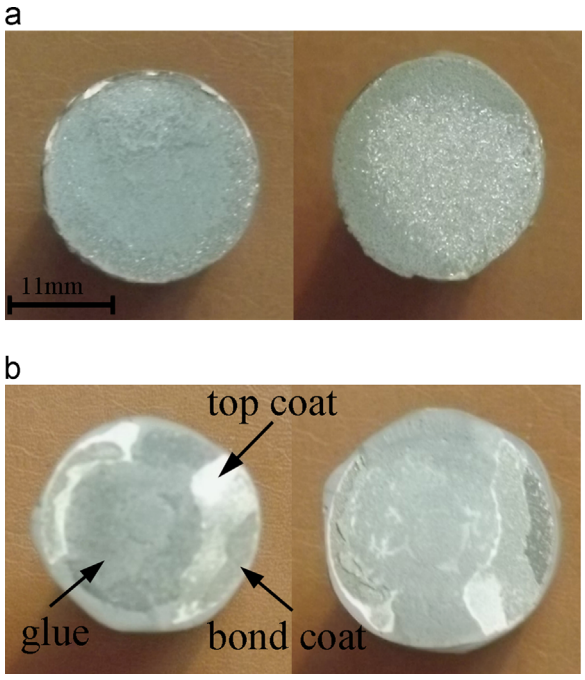

Fig. 7. Fractured surface of a TBC system after bonding strength test, (a) failure in the glued joint and (b) failure in the top coat-bond coat interface.

Table 3
Coating systems adhesion and failure location in ASTM-C633.

Sample	Strength bonding		Mode of fracture	
	Conventional coating	Nanostructured coating	Conventional coating	Nanostructured coating
1	28.25	40.28	b	b
2	12.20	31.04	a	b
3	22.05	45.00	b	b
4	21.30	18.30	b	a
5	26.80	36.16	b	b
Mean value	24.60	38.12	–	–

tip, E_i is 1140 GPa, and the ϑ_i is 0.07. Poisson's ratio of the specimen ϑ_s is 0.3.

In the nanoindentation experiments, the hardness is usually derived from

$$H = \frac{P_{\max}}{A} \tag{4}$$

where A is the actual contact area that can be obtained from Eq. (2) [55–58].

The hardness, H, and the Young's modulus, E, were determined from each measured unloading curve. As can be seen, the scatters in the resultant H and E were significantly large: H of conventional and nanostructured TBC varied from 5.874 to 11.001 and 5.531 to 16.019 GPa, respectively, and E of conventional and nanostructured TBC varied from 106.71 to 188.29 and 85.233 to 202.94 GPa, respectively. The large scatters may be attributed to the difference between the load microstructural features in the locality of each indentation position [58]. By computing the average value, the elastic modulus values of nanostructured and conventional TBCs are 161.49 GPa and 141.66 GPa, and the hardness values of nanostructured and conventional TBCs are 11.64 GPa and 8.38 GPa, respectively.

As we know that hardness is usually defined as resistance to penetration, deformation, scratching and erosion and it reflects the splat-to-splat cohesion of thermal spray coating [59], the higher hardness of the nanostructured TBC, as compared to the conventional TBC, can be attributed to the coating microstructure. In nanostructured TBC, the presence of non-molten phase increases the resistance to deformation. Therefore, by controlling the microstructure, it would be possible to control the durability of TBC. This can be done by using controlled porosity, segmentation, micro-cracking, and residual stress. Splat-splat cohesion, microcracking, can also play a role in the elastic modulus of TBC. The higher bonding strength (splat–splat cohesion) of the nanostructured TBC, as compared to the conventional TBC, leads to increasing elastic modulus of nanostructured TBC [25,58,60].

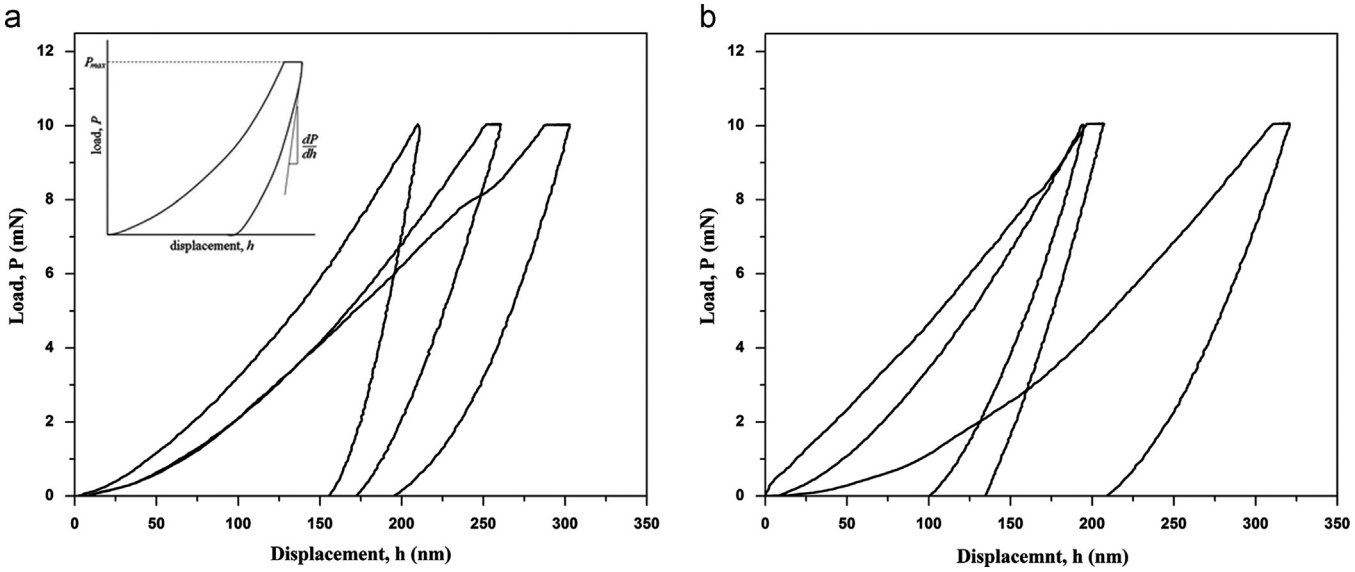

Fig. 8. Load versus indentation depth for indentation (a) conventional YSZ coating and (b) nanostructured YSZ coating.

Table 4
Summary of the best-fit values of nanoindentation test.

Sample	h_{max} (nm)		$S=dp/dh$ (mN/nm)		hc (nm)	
	Conventional coating	Nanostructured coating	Conventional coating	Nanostructured coating	Conventional coating	Nanostructured coating
1	260.66	207.21	0.1597	0.1760	212.53	162.29
2	209.81	194.13	0.2668	0.1568	181.37	145.85
3	302.54	320.37	0.1617	0.1382	256.61	265.59

4. Conclusion

In this study, microstructure, phase composition, and mechanical properties of nanostructured and conventional TBCs were investigated systematically; some important results can be summarized as follows:

1) The nanostructured as-sprayed coating possessed a lamellar structure consisting of nanosized particles retained from the powder and microcolumnar grains formed through the resolidification of the molten part of powder, while the microstructure of conventional coating consisted of columnar grain splats.
2) The results of XRD revealed that nanostructured coating only consisted of the non-transformable tetragonal phase, whereas the conventional coating consisted of the non-transformable tetragonal and monoclinic phases.
3) The presence of non-molten particles (nanozone) in the nanostructured coating could improve the bonding strength of TBCs.
4) Nanostructured TBCs had a hardness and Young's modulus higher than of those the conventional TBCs due to structural stability.

Acknowledgments

This work was supported by the Malek-Ashtar University of Technology, Department of Materials Engineering. The authors would like to gratefully thank the collaboration of Mrs. Raheleh Ahmadi-Pidani.

References

[1] M. Abbas, H. Guo, M.R. Shahid, Comparative study on effect of oxide thickness on stress distribution of traditional and nanostructured zirconia coating systems, Ceramics International 39 (2013) 475–481.
[2] Y. Li, Y. Xie, L. Huang, X. Liu, X. Zheng, Effect of physical vapor deposited Al_2O_3 film on TGO growth in YSZ/CoNiCrAlY coatings, Ceramics International 38 (2012) 5113–5121.
[3] M. Abbas, L. Guo, H. Guo, Evaluation of stress distribution and failure mechanism in lanthanum–titanium–aluminum oxides thermal barrier coatings, Ceramics International (2012), http://dx.doi.org/10.1016/j.ceramint.2012.12.006.
[4] N. Wang, C. Zhou, S. Gong, H. Xu, Heat treatment of nanostructured thermal barrier coating, Ceramics International 33 (2007) 1075–1081.
[5] C.R.C. Lima, N Cinca, J.M Guilemany, Study of the high temperature oxidation performance of thermal barrier coatings with HVOF sprayed bond coat and incorporating a PVD ceramic interlayer, Ceramics International 38 (2012) 6423–6429.
[6] S. Das, S. Datta, D. Basu, G.C. Das, Thermal cyclic behavior of glass–ceramic bonded thermal barrier coating on nimonic alloy substrate, Ceramics International 35 (2009) 2123–2129.
[7] L. Wang, Y. Wang, X.G. Sun, J.Q. He, Z.Y. Pan, C.H. Wang, Thermal shock behavior of 8YSZ and double-ceramic-layer $La_2Zr_2O_7$/8YSZ thermal barrier coatings fabricated by atmospheric plasma spraying, Ceramics International 35 (2012) 3595–3606.
[8] Y. Bai, L. Zhao, J.J. Tang, S.Q. Ma, C.H. Ding, J.F. Yang, L. Yu, Z.H. Han, Influence of original powders on the microstructure and properties of thermal barrier coatings deposited by supersonic atmospheric plasma spraying, part II: Properties, Ceramics International 39 (2013) 4437–4448.
[9] H. Jamali, R. Mozafarinia, R. Shoja-Razavi, R. Ahmadi-Pidani, Comparison of thermal shock resistances of plasma-sprayed nanostructured and conventional yttria stabilized zirconia thermal barrier coatings, Ceramics International 38 (2012) 6705–6712.
[10] L. Sun, H. Guo, H. Peng, S. Gong, H. Xu, Influence of partial substitution of Sc_2O_3 with Gd_2O_3 on the phase stability and thermal conductivity of Sc_2O_3-doped ZrO_2, Ceramics International 39 (2013) 3447–3451.
[11] P.G. Klemens, M. Gell, Thermal conductivity of thermal barrier coatings, Materials Science and Engineering: A 245 (1998) 143–149.
[12] C. Zhou, N. Wang, Z. Wang, S. Gong, H. Xu, Thermal cycling life and thermal diffusivity of a plasma-sprayed nanostructured thermal barrier coating, Scripta Materialia 51 (2004) 945–948.
[13] R.G. Hutchinson, N.A. Fleck, A.C.F. Cocks, A sintering model for thermal barrier coatings, Acta Materialia 54 (2006) 1297–1306.
[14] X.Q. Cao, R. Vassen, D. Stoever, Ceramic materials for thermal barrier coatings, Journal of the European Ceramic Society 24 (2004) 1–10.
[15] M.R. Begley, H.N.G. Wadley, Delamination resistance of thermal barrier coatings containing embedded ductile layers, Acta Materialia 60 (2012) 2497–2508.
[16] S. Guo, Y. Kagawa, Isothermal and cycle properties of EB-PVD yttria-partially stabilized zirconia thermal barrier coatings at 1150 and 1300 °C, Ceramics International 33 (2007) 373–378.
[17] R. Rajendran, Gas turbine coatings: an overview, Engineering Failure Analysis 26 (2012) 355–369.
[18] Y. Bai, Z.H. Han, H.Q. Li, C. Xu, Y.L. Xu, Z. Wang, C.H. Ding, J.F. Yang, High performance nanostructured ZrO_2 based thermal barrier coatings deposited by high efficiency supersonic plasma spraying, Applied Surface Science 257 (2011) 7210–7216.
[19] L. Pawlowski, The Science and Engineering of Thermal Spray Coating, Second ed., John Wiley & Sons, New York, 2008.
[20] Y. Zhang, J. Malzbender, D.E. Mack, M.O. Jarligo, X. Cao, Q. Li, R. Vaßen, D. Stöver, Mechanical properties of zirconia composite ceramics, Ceramics International (2012)http://dx.doi.org/10.1016/j.ceramint.2013.03.014.
[21] C.R.C. Lima, J.M. Guilemany, Adhesion improvements of thermal barrier coatings with HVOF thermally sprayed bond coats, Surface and Coatings Technology 201 (2007) 4694–4701.
[22] M. Okazaki, S. Yamagishi, Y. Yamazaki, K. Ogawa, H. Waki, M. Arai, Adhesion strength of ceramic top coat in thermal barrier coatings subjected to thermal cycles: effects of thermal cycle testing method and

environment, International Journal of Fatigue (2012)http://dx.doi.org/10.1016/j.ijfatigue.2012.02.014.
[23] L. Wang, Y. Wang, X.G. Sun, Z.Y. Pan, J.Q. He, C.G. Li, Influence of pores on the surface microcompression mechanical response of thermal barrier coatings fabricated by atmospheric plasma spray: finite element simulation, Applied Surface Science 257 (2011) 2238–2249.
[24] A. Dey, R.U. Rani, H.K Thota, A.K. Sharma, P. Bandyopadhyay, A.K. Mukhopadhyay, Microstructural, corrosion and nanomechanical behaviour of ceramic coatings developed on magnesium AZ31 alloy by micro arc oxidation, Ceramics International 39 (2013) 3313–3320.
[25] L. Wang, Y. Wang, X.G. Su, J.Q. He, Z.Y. Pan, C.H. Wang, Microstructure and indentation mechanical properties of plasma sprayed nano-bimodal and conventional ZrO_2–8wt%Y_2O_3 thermal barrier coatings, Vacuum 86 (2012) 1174–1185.
[26] N. Vecchione, K. Wasmer, D.S. Balint, K. Nikbin, Characterization of EB-PVD yttrium-stabilised zirconia by nanoindentation, Surface and Coatings Technology 203 (2009) 1743–1747.
[27] R.S. Lima, B.R. Marple, Enhanced ductility in thermally sprayed titania coating synthesized using a nanostructured feedstock, Materials Science and Engineering: A 395 (2005) 269–280.
[28] W.B. Gong, C.K. Sha, D.Q. Sun, W.Q. Wang, Microstructures and thermal insulation capability of plasma-sprayed nanostructured ceria stabilized zirconia coatings, Surface and Coatings Technology 201 (2006) 3109–3115.
[29] B. Liang, C. Ding, Thermal shock resistances of nanostructured and conventional zirconia coatings deposited by atmospheric plasma spraying, Surface and Coatings Technology 197 (2005) 185–192.
[30] H. Chen, X. Zhou, C. Ding, Investigation of the thermomechanical properties of a plasma-sprayed nanostructured zirconia coating, Journal of the European Ceramic Society 23 (2003) 1449–1455.
[31] L. Jin, L. Ni, Q. Yu, A. Rauf, C. Zhou, Thermal cyclic life and failure mechanism of nanostructured 13 wt%Al_2O_3 doped YSZ coating prepared by atmospheric plasma spraying, Ceramics International 38 (2012) 2983–2989.
[32] S. Bose, High Temperature Coatings, Elsevier Science & Technology Books, Connecticut, USA, 2007.
[33] G.D. Girolamo, C. Blasi, L. Pilloni, M. Schioppa, Microstructural and thermal properties of plasma sprayed mullite coatings, Ceramics International 36 (2010) 1389–1395.
[34] R.C. Reed, The Superalloys, Fundamentals and Applications, Cambridge University Press, Cambridge, 2006.
[35] H.W. Grunling, W. Mannsmann, Plasma sprayed thermal barrier coatings for industrial gas turbines: morphology, processing and properties, Journal of Physics IV 3 (1993) 903–912.
[36] H. Jamali, R. Mozafarinia, R. Shoja Razavi, R. Ahmadi-Pidani, M.R. Loghman-Estarki, Fabrication and evaluation of plasma-sprayed nanostructured and conventional YSZ thermal barrier coatings, Current Nanoscience 8 (2012) 402–409.
[37] H. Zhou, F. Li, B. He, J. Wang, B.D. Sun, Nanostructured yttria stabilized zirconia coatings deposited by air plasma spraying, Transactions of Nonferrous Metals Society 17 (2007) 389–393.
[38] O. Racek, C.C. Berndt, D.N. Guru, J. Heberlein, Nanostructured and conventional YSZ coatings deposited using APS and TTPR techniques, Surface and Coatings Technology 201 (2006) 338–346.
[39] R. Ahmadi-Pidani, R. Shoja-Razavi, R. Mozafarinia, H. Jamali, Improving the thermal shock resistance of plasma sprayed CYSZ thermal barrier coatings by laser surface modification, Optics and Lasers in Engineering 50 (2012) 780–786.
[40] H. Jamalin, R. Mozafarinia, R. Shoja-Razavi, R. Ahmadi-Pidani, Comparison of thermal shock resistances of plasma-sprayed nanostructured and conventional yttria stabilized zirconia thermal barrier coatings, Ceramics International 38 (2012) 6705–6712.
[41] H. Chen, Y. Zeng, C. Ding, Microstructural characterization of plasma-sprayed nanostructured zirconia powders and coatings, Journal of the European Ceramic Society 23 (2003) 491–497.
[42] J. Wu, H Guo, L. Zhou, L. Wang, S Gong, Microstructure and thermal properties of plasma sprayed thermal barrier coatings from nanostructured YSZ, Journal of Thermal Spray Technology 19 (2010) 1186–1195.
[43] G.D. Girolamo, F. Marra, C. Blasi, E. Serra, T. Valente, Microstructure, mechanical properties and thermal shock resistance of plasma sprayed nanostructured zirconia coatings, Ceramics International 37 (2011) 2711–2717.
[44] D. Seo, K. Ogawa, T. Shoji, S. Murata, Effect of particle size distribution on isothermal oxidation characteristics of plasma sprayed CoNi- and CoCrAlY coatings, Journal of Thermal Spray Technology 16 (2007) 954–966.
[45] J. Sun, L. Zhang, D. Zhao, Microstructure and thermal cycling behavior of nanostructured yttria partially stabilized zirconia (YSZ) thermal barrier coatings, Journal of Rare Earths 28 (2010) 198–201.
[46] X. Jiang, C. Liu., F. Lin, Overview on the development of nanostructured thermal barrier coatings, Journal of Materials Science &Technology 23 (2007) 449–457.
[47] R.S. Lima, B.R. Marple, Thermal spray coatings engineered from nanostructured ceramic agglomerated powders for structural, thermal barrier and biomedical applications: a review, Journal of Thermal Spray Technology 16 (2007) 40–63.
[48] R.S. Lima, A Kucuk, C.C. Berndt, Integrity of nanostructured partially stabilized zirconia after plasma spray processing, Materials Science and Engineering: A 313 (2001) 75–82.
[49] R. Mcpherson, A review of microstructure and properties of plasma sprayed ceramic coatings, Surface and Coatings Technology 39–40 (1989) 173–181.
[50] H. Chen, C. Ding, S. Lee, Phase composition and microstructure of vacuum plasma sprayed nanostructured zirconia coating, Materials Science and Engineering: A 361 (2003) 58–66.
[51] B. Liang, C. Ding, H. Liao, C. Coddet, Phase composition and stability of nanostructured 4.7 wt% yttria-stabilized zirconia coatings deposited by atmospheric plasma spraying, Surface and Coatings Technology 200 (2006) 4549–4556.
[52] B. Liang, C. Ding, Phase composition of nanostructured zirconia coatings deposited by air plasma spraying, Surface and Coatings Technology 191 (2005) 267–273.
[53] A. Hjorhhede, A. Nylund, Adhesion testing of thermally sprayed and laser deposited coatings, Surface and Coatings Technology 28 (2004) 208–218.
[54] M. Gell, E.H. Jordan, Y.H. Sohn, D. Goberman, L. Shaw, T.D. Xiao, Development and implementation of plasma sprayed nanostructured ceramic coatings, Surface and Coatings Technology 146–147 (2001) 48–54.
[55] B. Poon, D. Rittel, G. Ravichandran, An analysis of nanoindentation in linearly elastic solids, International Journal of Solids and Structures 45 (2008) 6018–6033.
[56] S. Guo, Y. Kagawa, Effect of loading rate and holding time on hardness and Young's modulus of EB-PVD thermal barrier coating, Surface and Coatings Technology 182 (2004) 92–100.
[57] S. Guo, Y. Kagawa, Effect of thermal exposure on hardness and Young's modulus of EB-PVD yttria-partially-stabilized zirconia thermal barrier coatings, Ceramics International 32 (2006) 263–270.
[58] R.S. Lima, A. Kucuk, C.C. Berndt, Bimodal distribution of mechanical properties on plasma sprayed nanostructured partially stabilized zirconia, Materials Science and Engineering: A 327 (2002) 224–232.
[59] K.M. Amin, Toughness, hardness, and wear, Engineered Materials handbook, in: S.J. Schneider (Ed.), Ceramic and Glasses, 4, ASM International, 1991, pp. 599–609.
[60] A. Keyvani, M. Saremi, M. Heydarzadeh-Sohi, An investigation on oxidation, hot corrosion and mechanical properties of plasma-sprayed conventional and nanostructured YSZ coatings, Surface and Coatings Technology 206 (2011) 208–216.